

Atomic short-range order and alloy ordering tendency in the Ag-Au system

This content has been downloaded from IOPscience. Please scroll down to see the full text.

1995 Modelling Simul. Mater. Sci. Eng. 3 753

(<http://iopscience.iop.org/0965-0393/3/6/002>)

View [the table of contents for this issue](#), or go to the [journal homepage](#) for more

Download details:

IP Address: 128.138.41.170

This content was downloaded on 14/07/2015 at 11:35

Please note that [terms and conditions apply](#).

Atomic short-range order and alloy ordering tendency in the Ag–Au system

Z W Lu†, Barry M Klein† and Alex Zunger‡

† Department of Physics, University of California, Davis, CA 95616, USA

‡ National Renewable Energy Laboratory, Golden, CO 80401, USA

Received 28 February 1995, accepted for publication 29 May 1995

Abstract. Accurate information of energetics is essential to map out the temperature versus composition phase diagram of a binary substitutional $A_{1-x}B_x$ alloy. Since it is computationally prohibitive to calculate the total energies of all 2^N configurations obtained by occupying N sites by A and B atoms, we map instead the *ab initio* calculated total energies of only $O(10)$ simple structures (with ≤ 8 atoms/cell) onto a generalized Ising model (including pair and many-body interactions) finding that for Ag–Au a close reproduction (within ~ 2 meV/atom) of LDA energies of *arbitrary structures* can be achieved by including relatively short-ranged interactions. Subjecting these Ising interaction parameters to a Monte Carlo simulated annealing treatment, we obtain (i) the structures having $T = 0$ minimum energy ('ground states'); (ii) the order–disorder phase transition temperatures; (iii) the mixing enthalpy for the disordered alloy; and (iv) the high-temperature atomic short-range order (SRO). While the predicted ordering temperatures for the ground state structures are too low to enable direct growth into the ordered phase, the calculated mixing enthalpy and the SRO parameters for Ag–Au agree quantitatively with experiment and clearly indicate a tendency for ordering, not phase separation.

1. Introduction

Theoretical calculations of temperature–composition phase diagrams of $A_{1-x}B_x$ alloys are needed for (i) *verification* [1–3] of existing measurements for low-temperature phases and of order–disorder transition temperatures; (ii) *predictions* [4–6] of hitherto unsuspected ordered structures missed by experimentalists; and (iii) *development of understanding* [4, 7] of the electronic and structural origins of phase stability. Under class (i) we note the calculation of phase diagrams for III–V and II–VI semiconducting alloys [1, 2], and noble-metal alloys [3, 4]. Under class (ii) we mention the recent prediction [5] of the Ni_7Al structure in $Ni_{1-x}Al_x$ alloys; the $L1_2$ (Pd_3Pt), $L1_0$ ($PdPt$), and $L1_2$ ($PdPt_3$) structures in $Pd_{1-x}Pt_x$ alloys; and superlattices stacked along the [012] directions in $Rh_{1-x}Pt_x$ alloys [8]. Under class (iii) we note the discovery that scalar–relativistic effects (mass–velocity and Darwin term) are a major contributions to ordering in Ni–Pt [7] and phase separation in Au–Pt [7]; that spin polarization stabilizes the $L1_2$ structure in Pd_3Cr , Pt_3Cr , and Pd_3Fe [9]; and that atomic size differences in Ni–Au and GaP–InP lead to phase-separating low-temperature ground states, but with an ordering-type short-range order at high temperatures [10].

Phase diagrams and order–disorder phenomena in binary $A_{1-x}B_x$ substitutional alloys can be studied theoretically by mapping atoms A and B onto a spin- $\frac{1}{2}$ generalized Ising model [11, 12]. In such a model one assigns (1) a set of 'spin' variables \hat{S}_i ($i = 1, 2, \dots, N$) to each of the N sites of the lattice, with $\hat{S}_i = -1$ (+1) if site i is occupied by an A (B)

atom, and (2) a set of interaction energies $\{J_F\}$ among the various sites belonging to a 'figure' F (pairs, triplets, quadruplets, etc). A configuration σ is defined as a particular set of occupations of each of the N lattice sites by an A (or a B) atom. The total energy $E(\sigma)$ for any configuration σ can be rigorously cluster expanded (CE) as

$$E_{\text{CE}}(\sigma) = J_0 + \sum_i J_i \hat{S}_i(\sigma) + \sum_{j<i} J_{ij} \hat{S}_i(\sigma) \hat{S}_j(\sigma) + \sum_{k<j<i} J_{ijk} \hat{S}_i(\sigma) \hat{S}_j(\sigma) \hat{S}_k(\sigma) + \dots \quad (1)$$

where $\{J_F\}$ are the interaction energies, and the summations are over all sites in the lattice; over 'figures' F containing all pairs of sites; and over all triplets, and so on. The interaction energies $\{J_F\}$ are the same for all configurations σ . In the traditional approach [13,14] one assumes *a priori* an interaction range (usually a short-ranged pair interaction) and extracts the Ising interaction parameters by fitting [13,14] them to the experimentally determined phase diagrams [14] or to the experimentally determined diffuse-scattering intensities [15,16]. Recent first-principles alloy theories (reviewed in [11,12]) instead extract these Ising interaction energies directly from the *ab initio* calculated total energies of a small set $\{\sigma\}$ of ordered configurations: the basic idea is that if the series of equation (1) converges reasonably rapidly (in practice, 10–20 terms are needed), these energies J_F can be obtain by inverting [17] or least-square fitting [5] equation (1) to a set of (10–20) total energies $\{E_{\text{direct}}(\sigma)\}$ of structures $\{\sigma\}$ calculated directly from e.g., using the local density approximation (LDA) [18]. Because the Ising representation of the energy is a linear function of J_F and the spin products, once $\{J_F\}$ is known one can readily use equation (1) to predict the total energy of *any of the* 2^N configurations. One can further calculate temperature-dependent physical properties using statistical mechanics techniques [11]. The predictions from these first-principles cluster expansion methods have met with not only qualitative but in many cases also quantitative agreement with experiment [11,12].

A successful alloy theory depends critically on its ability to accurately reproduce the alloy energetics, since the temperature versus composition phase diagram represent a delicate balance between structures with nearly equal energies. For a fixed type of lattice with N sites, there are 2^N substitutional configurations for binary $A_{1-x}B_x$ alloys. It is obviously impossible to calculate the total energies of such a large number of configurations using self-consistent, first-principle LDA methods, whose computational efforts increase rapidly ($\propto M^3$) with the number of atoms M in the unit cell. However, a cluster-expanding physical quantity in terms of Ising-like interaction requires but 10–20 total energy calculations, yet it enables prediction of 2^N total energies. Thus, this approach extends the applicability of first-principles total energy calculations from structures with cells containing a small number of atoms (~ 10) to a large number of structurally complex substitutional configurations, including random alloys, alloys with short-range order, superlattices, and antiphase boundaries, many of which are computationally too complex to be treated using current first-principles methods. For systems consisting of atoms with very different sizes, the atoms often move off their ideal lattice sites ('relaxation') causing a slowing down in the convergence of the cluster expansion [19–21]. The recently developed [19] mixed-space cluster expansion, which sums an infinite series of pair interactions cast in reciprocal space (treating all other interactions in real space), has overcome this problem. It predicted the correct $T = 0$ ground state structures, the mixing enthalpies, and the diffuse-scattering intensities of Cu–Pd and GaP–InP systems [19,22].

We selected the Ag–Au system for our study because there is a wealth of previous theoretical and experimental data on this system to compare with.

(i) Solid state mixing enthalpy has been measured [23] and also has been calculated using empirical methods [24–26] and first-principles methods in junction with the cluster

expansion techniques [1, 27–30].

(ii) Electronic structure and charge transfer effects have been investigated both experimentally [31–34] and theoretically [35–39].

(iii) The short-range order has been measured by a number of groups [15, 40, 41]. The recent careful measurement and analysis of SRO [15] has prompted us to make a direct comparison between theory and experiment.

(iv) The recent explosion of interest in metallic superlattices (including the Ag–Au system [42–47]) has given us added reason to investigate this system.

The Ag–Au system is particularly convenient for the cluster expansion method, since the elemental face-centered cubic Ag and Au constituents have nearly the same measured room-temperature lattice constants [48] (4.086 and 4.078 Å for Ag and Au, respectively), so there is no slowing down of the convergence of the cluster expansion. In this paper, we demonstrate how we obtain accurate alloy properties of Ag–Au using as input a reasonably small number of first-principles LDA total energy calculations. Specifically, we will show how we (i) select structures for LDA total energy calculations; (ii) select the interaction figures for the cluster expansion; (iii) test the convergence of the cluster expansion; (iv) use the Monte Carlo [49–51] simulated annealing [52] technique to predict the low-temperature ground state structures and the order–disorder phase transition temperatures; (v) compare the calculated and experimental mixing energy for the disordered alloy; and (vi) compare the calculated and experimental short-range order parameters.

2. Method of calculation

The excess energy (or low-pressure enthalpy) $\Delta E(\sigma, V)$ of any substitutional configuration σ is given by

$$\Delta E_{\text{direct}}(\sigma, V) = E(\sigma, V) - [(1-x)E_A(V_A) + xE_B(V_B)] \quad (2)$$

with the volume, V , dependence and is defined with respect to the energies of equivalent amounts of the pure solids A and B at their respective equilibrium volumes, V_A and V_B . The low-temperature long-range order (LRO) of a given lattice type is then interpreted as the configuration σ which gives the lowest $\Delta E_{\text{direct}}(\sigma, V_\sigma)$ at the equilibrium volume V_σ . One can cluster expand (CE) the directly calculated $\Delta E_{\text{direct}}(\sigma, V)$ in a finite Ising-like series as in equation (1). By taking advantage of symmetry properties, the terms in equation (1) can be further grouped together in a concise form:

$$\Delta E_{\text{CE}}(\sigma, V) = \sum_F D_F J_F(V) \overline{\Pi}_F(\sigma) \quad (3)$$

where $J_F(V)$ are volume-dependent interaction energies of basic lattice figures F , e.g., nearest-neighbor pairs, next-neighbor pairs, triangles, etc. Figure 1 shows examples of some of these figures on a fcc lattice. The ‘lattice-averaged spin products’ $\overline{\Pi}_F(\sigma)$ are the product over *all* the figures f (related to F) of the variables \hat{S}_i , averaged over all symmetry equivalent figures of the lattice. D_F is the degeneracy of the figure F . Since in the Ag–Au system the lattice mismatch ($a_A - a_B$) is very small, we will ignore the volume dependence in equation (3), using instead $\bar{V} = (V_A + V_B)/2$ or a cubic lattice constant $\bar{a} = 4.032$ Å. All of the terms on the right-hand side of equation (3) are trivially determined geometrical quantities, with the exception of J_F , the effective interaction energies. Since $\{\overline{\Pi}_F(\sigma)\}$ is a complete, orthonormal set of polynomials, the expansion equation (3) is exact [53], if not truncated. In practice, one hopes that this series converges reasonably rapidly, so only $N_J \sim O(10)$ interactions are retained (the first few pair interactions, as well as several

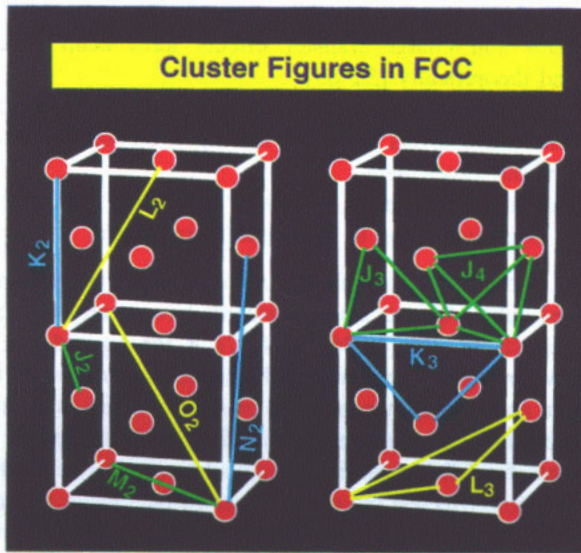


Figure 1. Geometric figures used in our cluster expansion. The expansion includes pair figures, three-body figures, and four-body figures. See table 3 for the definition of the figure coordinates.

many-body terms). We determine the N_J interaction parameters $\{J_F\}$ by mapping N_σ directly calculated $\Delta E_{\text{direct}}(\sigma)$ values onto $\Delta E_{\text{CE}}(\sigma)$ of equation (3) through a least-squares fitting procedure, i.e., by minimizing

$$\sum_{\sigma_s}^{N_\sigma} |\Delta E_{\text{direct}}(\sigma_s) - \Delta E_{\text{CE}}(\sigma_s)|^2 = \min \quad (4)$$

where $N_\sigma \geq N_J$. Convergence is tested by applying equation (3) to a set of structures $\{\sigma'\}$ not used in constructing the cluster expansion of equation (4). We define the prediction error (PE) as

$$\delta_{\text{PE}}(\sigma') = E_{\text{direct}}(\sigma') - E_{\text{CE}}(\sigma'). \quad (5)$$

If the prediction errors are larger than a prescribed tolerance, more many-body figures and input structures are added to the expansion of equation (3).

We have calculated the total energy versus volume $E(V)$ for the elemental fcc solids Ag and Au using the LDA-based full-potential linearized augmented plane wave (LAPW) method [54, 55]. We have used the LDA exchange correlation potential of Ceperley and Alder [56], as parametrized by Perdew and Zunger [57], and have used 60 special k -points [58] in performing the k -space summations. The calculated equilibrium fcc lattice parameters of the pure Ag and Au are 4.008 Å and 4.056 Å, compared with the room-temperature experimental data [48] of 4.086 Å and 4.078 Å, respectively. LDA thus underestimates the lattice parameters of Ag and Au by 1.9% and 0.5%, respectively. Our current lattice parameters are nearly the same as those calculated using the LAPW method by Klein and Fong [39], but are slightly different from those calculated previously using the LAPW method by Wei *et al* [3], yielding 4.057 Å and 4.105 Å for Ag and Au, respectively. The difference between the present results and those of Wei *et al* is due mainly to a different exchange–correlation potential (Wigner form) [59] used in [3]. We have calculated the excess total energies $\Delta E_{\text{direct}}(\sigma, \bar{V})$ of equation (2) for $N_\sigma = 32$ ordered structures $\{\sigma\}$ involving a small number of atoms in the unit cell (up to 8 atoms/cell) [5]. Figure 2 shows

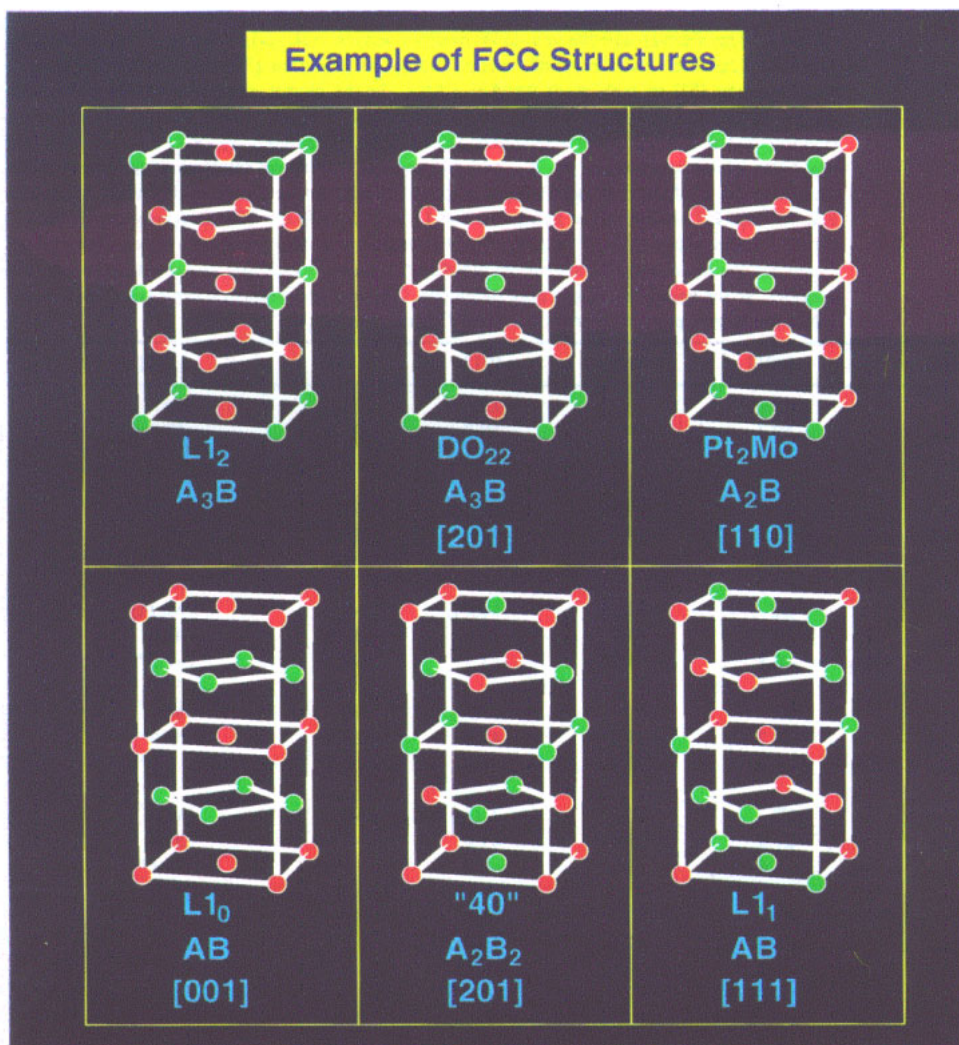


Figure 2. Examples of some simple, fcc-based structures used in this work: the $L1_2$ structure (prototype Cu_3Au); the DO_{22} (prototype Al_3Ti); prototype Pt_2Mo structure; the $L1_0$ (prototype $CuAu-I$); structure '40' in [61]; and the $L1_1$ structure (prototype $CuPt$). Some of these structures are superlattices along some orientation (see table 1).

examples of some simple fcc-based ordered structures used in our calculations. Table 1 and its caption define these structures. Most of these structures can be described as short-period A_mB_n superlattices along some orientation as shown in figure 2 and table 1. The calculations for ordered compounds are all carried out at the average cubic lattice constant of $\bar{a} = 4.032 \text{ \AA}$, and the atoms are assumed to be on their ideal fcc positions since the effects of lattice relaxation on ΔH are small here (e.g., for Ag–Au, relaxation lowers the energy of the $L1_0$ structure by less than 1.5 meV/atom. For comparison, in the 12% size-mismatched Cu–Au system relaxation lowers the energy of the $L1_0$ structure by ~ 13 meV/atom). To obtain highly precise results we use a k -point sampling scheme that is geometrically equivalent

Table 1. The directly calculated LAPW excess energies $\Delta E_{\text{direct}}(\sigma)$ (error $\sim \pm 2$ meV/atom) (equation (2)), the cluster-expanded energy $\Delta E_{\text{CE}}(\sigma)$ (equation (3)), and the prediction error δ_{PE} (equation (5)) in meV/atom for $\text{Ag}_{1-x}\text{Au}_x$. In the cluster expansion (fit 1) we include $N_\sigma = 18$ ordered structures and $N_f = 12$ interaction energies. These include the reference (empty) interaction J_0 , point interaction J_1 , six pair interactions, J_2, K_2, L_2, M_2, N_2 , and O_2 , three triplet interactions, J_3, K_3 , and L_3 , and one quadruplet interaction J_4 . Many of the structures can be defined as superlattices in given orientations, as shown in this table. Structures D1, D4, and D7 are defined in figures 10 and 11 in [5], while the SQS structures are defined in figure 1 and equations (2)–(4) in [38]. The $L1_2$ structure is also not a superlattice. The symbol * denotes the structures that are not included in our cluster expansion to extract the interaction energies, so the energy value is a pure prediction. The average prediction error is 1.0 meV/atom, while the largest prediction error is 1.8 meV/atom.

Formula	[001]	[011]	[012]	[111]	[113]
AB	$L1_0$	$L1_0$	$L1_0$	$L1_1$	$L1_1$
ΔE_{direct}	-59.7	-59.7	-59.7	-43.0	-43.0
$\Delta E_{\text{direct}} - \Delta E_{\text{CE}}$	-0.4	-0.4	-0.4	0.4	0.4
A_2B	$\beta 1$	MoPt ₂	MoPt ₂	$\alpha 1$	MoPt ₂
ΔE_{direct}	-40.8	-49.7	-49.7	-30.2	-49.7
$\Delta E_{\text{direct}} - \Delta E_{\text{CE}}$	-0.4	-1.7*	-1.7*	-0.5	-1.7*
AB_2	$\beta 2$	MoPt ₂	MoPt ₂	$\alpha 2$	MoPt ₂
ΔE_{direct}	-40.0	-46.9	-46.9	-30.8	-46.9
$\Delta E_{\text{direct}} - \Delta E_{\text{CE}}$	-0.8	-1.3*	-1.3*	-0.5	-1.3*
A_3B	Z1	Y1	DO_{22}	V1	W1
ΔE_{direct}	-29.2	-37.0	-42.3	-21.3	-35.9
$\Delta E_{\text{direct}} - \Delta E_{\text{CE}}$	1.0	0.4	0.0	0.7*	1.4*
AB_3	Z3	Y3	DO_{22}	V3	W3
ΔE_{direct}	-27.9	-35.4	-41.0	-21.4	-34.4
$\Delta E_{\text{direct}} - \Delta E_{\text{CE}}$	1.4	0.8	-0.2	1.0*	0.1*
A_2B_2	Z2	Y2	'40'	V2	W2
ΔE_{direct}	-28.8	-44.1	-55.3	-22.9	-50.6
$\Delta E_{\text{direct}} - \Delta E_{\text{CE}}$	1.2	-0.1	-0.4*	-0.1*	-0.4*
Non-superlattice	$L1_2$ (A_3B)	$L1_2$ (AB_3)	Ag	Au	
ΔE_{direct}	-43.4	-44.0	0.0	0.0	
$\Delta E_{\text{direct}} - \Delta E_{\text{CE}}$	0.0	0.1	-0.3	-0.4	
Non-superlattice	D1 (A_7B)	D4 (A_4B_4)	D7 (AB_7)	SQS8 _a (A_4B_4)	SQS8 _b (A_4B_4)
ΔE_{direct}	-20.8	-42.9	-20.0	-42.5	-43.6
$\Delta E_{\text{direct}} - \Delta E_{\text{CE}}$	1.8	1.1	0.6	0.5	-0.1

in the compound and its pure constituents [60], leading to, e.g., the total energy of A_3A in the $L1_2$ or DO_{22} crystal structures being equal to the fcc value (A). In practice we use sets of k -points that are equivalent to 408 fcc special k -points [58]: increasing the equivalent k -points from 60 to 408, the energy of each structure changes by less than 1 meV/atom, except for the Y1 and Y2 structures for which the changes are 1.2 and 1.6 meV/atom, respectively. Table 2 shows the effects of k -point sampling on ΔE_{direct} for a few structures. We also use a large basis set cut-off of $R_{\text{MT}}K_{\text{max}} = 9.0$ ($R_{\text{MT}}^{\text{Ag}} = R_{\text{MT}}^{\text{Au}} = 2.55$ au), which corresponds to ~ 85 LAPWs/atom. In the LAPW calculations, the core states are treated

Table 2. This table illustrates the effects of k -point sampling on the calculated ΔE_{direct} (in meV/atom) of some ordered compounds. The structures are defined in table 1. We have used the equivalent k -point sampling scheme of [60]; these two k -point sets are equivalent to 60 and 408 fcc special k -points, respectively (see [58]). We also give the actual number of k -points, N_k , in the irreducible zone for a particular structure.

Structure	Formula	60 equiv. fcc k -points		408 equiv. fcc k -points	
		N_k	ΔE_{direct}	N_k	ΔE_{direct}
W1	Ag ₃ Au	136	−36.2	1056	−35.9
Y1	Ag ₃ Au	88	−35.8	608	−37.0
Y2	Ag ₂ Au ₂	88	−42.5	608	−44.1
W2	Ag ₂ Au ₂	136	−51.0	1056	−50.6
L1 ₀	AgAu	80	−60.7	576	−59.7
Y3	AgAu ₃	88	−34.8	608	−35.4
W3	AgAu ₃	136	−35.1	1056	−34.4

fully relativistically, while the valence states are treated scalar-relativistically, ignoring the spin–orbit interaction (its effect on ΔH is rather small). The total error in ΔE_{direct} is estimated to be ~ 2 meV/atom, which is comparable to the energy of the zero-point motion.

Once a converged cluster expansion of equation (3) is established, we can use it to calculate the properties of the ideally ($T \rightarrow \infty$) random alloys. Denoting a configurational average for the ideally random (R) state by angular brackets $\langle \rangle_R$ the mixing enthalpy of the random alloy is

$$\Delta H_{\text{mix}}(x) \equiv \langle \Delta E_{\text{CE}}(\sigma) \rangle_R = \sum_F D_F J_F \langle \bar{\Pi}_F \rangle_R = \sum_F D_F J_F (2x - 1)^{k_F} \quad (6)$$

where $\langle \bar{\Pi}_F \rangle_R = (2x - 1)^{k_F}$ and k_F is the number of vertices in figure F , so that at $x = \frac{1}{2}$ and $T \rightarrow \infty$ we have

$$\Delta H_{\text{mix}}(x = \frac{1}{2}) = J_0. \quad (7)$$

The ordering energy of configuration σ measures the difference between the energy of σ and that of the random alloy with the same composition:

$$\delta E_{\text{ord}}(\sigma) \equiv \Delta E_{\text{CE}}(\sigma) - \langle \Delta E_{\text{CE}}(\sigma) \rangle_R = \sum_F D_F J_F [\bar{\Pi}_F(\sigma) - (2x - 1)^{k_F}]. \quad (8)$$

Also, using our set of $\{J_F\}$ we can calculate the lowest-energy ‘ground state structures’ by applying linear programming techniques [61, 62], or simply searching a large enough structural data base [5] to locate the lowest-energy structure using equation (3). We will use a Monte Carlo simulated annealing method [22, 52] to obtain simultaneously (i) the $T = 0$ ground state structures (on a finite cell), (ii) the order–disorder transition temperatures, (iii) finite-temperature short-range order (SRO) and energies of the disordered alloy. A Monte Carlo cell size of $16^3 = 4096$ atoms (with periodic boundary conditions) was used in our calculations. Monte Carlo simulated annealing was performed in the canonical ensemble at a fixed concentration, with the transition temperature being calculated from the discontinuity in the internal energy as a function of temperature, and the ground state determined by the state of the simulation at a temperature where all configurational changes proved to be energetically unfavorable. Since we ran the Monte Carlo simulation with decreasing temperature, it tends to supercool a structure. The resulting transition temperature is thus a lower bound of the real T_c . The estimated error is around 20 K for the present system.

The Warren–Cowley SRO parameter [63, 63] for the N th atomic shell at distance R_{lmn} from the origin is

$$\alpha_{\text{SRO}}(R_{lmn}) = \frac{\langle \bar{\Pi}_{0,N} \rangle - q^2}{1 - q^2} \quad (9)$$

where $q = 2x - 1$ and $\langle \bar{\Pi}_{0,N} \rangle$ is the configurational average of the pair correlation function between sites zero and N . Note that $\alpha_{\text{SRO}}(R_{000}) \equiv 1$ by definition. The Fourier transform of the real-space SRO is $\alpha_{\text{SRO}}(\mathbf{k})$, which is proportional to the diffuse intensity due to SRO. Its value depends on the number, N_R , of real-space shells used in the transform:

$$\alpha_{\text{SRO}}(\mathbf{k}, N_R) = \sum_N^{R_{lmn}} \alpha_{\text{SRO}}(R_{lmn}) e^{i\mathbf{k} \cdot \mathbf{R}_{lmn}}. \quad (10)$$

In the calculation of $\alpha_{\text{SRO}}(R_{lmn})$ and $\alpha_{\text{SRO}}(\mathbf{k}, N_R)$, 500 Monte Carlo steps per site are used to equilibrate the system (which is initialized to a completely random state), and subsequently averages are taken over 100 Monte Carlo steps per site. The values of N_R in our calculations are dictated by the number of experimental SRO parameters reported [15]. The absolute values of the SRO parameter increase as the annealing temperature is lowered. For Ag–Au, lowering the temperature at which our Monte Carlo simulation ($T = 600$ K) is performed by 100 K increases the values of the SRO parameter by less than 10%, which is similar to the experimental accuracy. The values of experimental SRO parameters are very sensitive to the experimental conditions: sample growth conditions, history of heat treatment etc. The experimental Ag–Au samples are homogenized at $T \sim 1200$ K and subsequently aged at $T \sim 500$ K; the samples probably reflect the state of thermodynamic equilibrium of a temperature somewhat above 500 K.

3. Results

3.1. LDA energies of ordered structures

The directly calculated excess enthalpies $\Delta E_{\text{direct}}(\sigma)$ are collected in table 1. One immediately notices that $\Delta E_{\text{direct}}(\sigma)$ are negative, unequivocally indicating ordering in this alloy system. Among this set of 32 structures, we find that the D1, $L1_2$, MoPt₂, $L1_0$, MoPt₂, $L1_2$, and D7 have the lowest energies at their respective compositions of $x = \frac{1}{8}, \frac{1}{4}, \frac{1}{3}, \frac{1}{2}, \frac{2}{3}, \frac{3}{4}$, and $\frac{7}{8}$. These structures could be the contenders for the ground states, but the ground state structure that we calculated by MC need not be in the input set. The D1 structure at $x = \frac{1}{8}$ can not be the ground state, since the energy of a linear combination of the nearby $L1_2$ structure at $x = \frac{1}{4}$ and the pure element at $x = 0$ is -21.7 meV/atom and is slightly lower in energy than the D1 structure energy of -20.8 meV/atom. Similarly, the D7 structure at $x = \frac{7}{8}$ can not be the ground state either, since the energy of a linear combination of the nearby $L1_2$ structure at ($x = \frac{3}{4}$) and the pure element at $x = 1$ is -22.0 meV/atom and is slightly lower in energy than the D7 structure energy of -20.0 meV/atom. Note that $\{\Delta E_{\text{direct}}(\sigma)\}$ does not show any systematic trend with σ that can be recognized. By extracting a set of interaction energies $\{J_F\}$ we will unravel the trends.

3.2. Cluster interaction energies

We will discuss three levels (in increasing order of complexity and accuracy) of choosing interaction energies. First, Connolly and Williams [17] (CW) proposed a cluster-expansion scheme to obtain the nearest-neighbor fcc interactions, J_0, J_1, J_2, J_3 , and J_4 defined in figure 1 from $N_\sigma = 5$ structures: the fcc elements A and B, $L1_2$ (A_3B and AB_3) and $L1_0$

(AB). Using this original Connolly–Williams procedure, we obtained an average prediction error of $\delta_{PE} = 1.6$ meV/atom and a maximum prediction error of 4.4 meV/atom for 27 other structures that are not used in obtaining the interaction J values. The prediction errors for some specific structures are unsatisfactory. For example δ_{PE} are 4.4, 2.4, 3.0, 2.6 meV/atom, for structures ‘40’, $\gamma 2$, DO_{22} ($AgAu_3$), and W3, respectively (larger than the estimated error of direct LDA calculation of 2 meV/atom). The large error for ‘40’ and DO_{22} is because the Connolly–Williams set of interactions creates a spurious degeneracy of the L_{10} and ‘40’ structures, and similarly for the L_{12} and DO_{22} structures.

Second, in addition to the Connolly and Williams set of five interactions, Lu *et al* [5] has added more pair interactions (K_2 , L_2 , and M_2) to the set. These eight interactions were obtained from fitting the energies of 12 structures: A, L_{12} , DO_{22} , $\beta 1$, L_{10} , L_{11} , ‘40’, Z2, $\beta 2$, L_{12} , DO_{22} , and B. Using this procedure, we obtained an average prediction error of $\delta_{PE} = 1.6$ meV/atom and a maximum prediction error of 4.0 meV/atom for 20 other structures that are not used in obtaining interaction J values. Here too, the prediction errors for many structures are also unsatisfactory, e.g. δ_{PE} are 2.2, 4.0, 3.1 meV/atom, for structures $\alpha 2$, $\gamma 1$, and Y2, respectively.

Third, figure 3 shows a converged set of interactions for Ag–Au obtained using 18 structures $\{\sigma\}$ in equation (4) (i.e., A, B, L_{10} , L_{12} , L_{12} , L_{11} , DO_{22} , DO_{22} , Z1, Z3, $\alpha 1$, $\alpha 2$, $\beta 1$, $\beta 2$, Y1, Y2, Y3, and W2). These include, the reference (empty) interaction J_0 , point interaction J_1 , six pair interactions, J_2 , K_2 , L_2 , M_2 , N_2 , and O_2 , three triplet interactions, J_3 , K_3 , and L_3 , and one quadruplet interaction J_4 . Table 3 gives the values of these interaction energies (denoted ‘fit I’), while figure 3 further shows that the nearest-neighbor pair interaction J_2 (table 3) is dominant, while other interactions are smaller by at least an order of magnitude. The average fitting error is 0.6 meV/atom and the maximum fitting error is 1.3 meV/atom. We have tested these interaction parameters by predicting ΔE_{direct} for 14 structures $\{\sigma'\}$ that are not used to obtain $\{J\}$ values. Compared with directly calculated LAPW values, we find an average prediction error of $\delta_{PE} = 1.0$ meV/atom, with a maximum prediction error of 1.8 meV/atom. This is illustrated in table 1 and is designated as ‘fit I’.

Finally, to test the sensitivity of the resulting interaction parameter to the input structures, we also used a set of 17 structures that have been used before for studying the Cu–Pd alloy [22]. These structures are A, B, L_{10} , L_{12} , L_{12} , ‘40’, L_{11} , Z2, DO_{22} , DO_{22} , Z1, Z3, $\alpha 1$, $\alpha 2$, $\beta 1$, V1, and D4 (we have only calculated total energies for structures containing ≤ 8 atoms/cell). The resulting interaction parameters (designated as ‘fit II’) shown in table 3 are very similar to those of ‘fit I’ above. Since we used fewer input structures in fit II (17) than in fit I (18), we also used two fewer pair interactions in fit II (10) than in fit I (12). Fit II has an average fitting error of 0.7 meV/atom for 17 structures used to extract the interaction energies $\{J\}$. We have tested these interaction parameters by predicting ΔE_{direct} for 15 structures $\{\sigma'\}$ that are not used to obtain $\{J\}$ values. Compared with directly calculated LAPW values, we find an average prediction error of $\delta_{PE} = 1.5$ meV/atom, with a maximum prediction error of 2.5 meV/atom. This fit is only slightly worse than fit I.

3.3. Mixing enthalpies of the disordered alloy

The mixing enthalpy of completely random alloy ($T \rightarrow \infty$) is given by equation (6). At $x = \frac{1}{2}$, it is given by equation (7). Using ‘fit I’ we find

$$\Delta H_{mix}(x = \frac{1}{2}) = -43.4 \text{ meV/atom.} \quad (11)$$

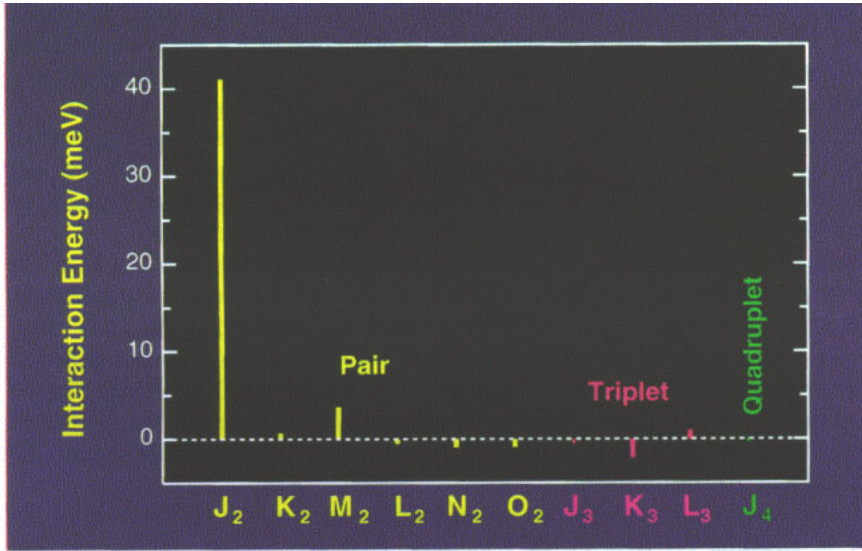


Figure 3. This figure illustrates the interaction energies (including the degeneracy $D_F J_F$) used in this work (figure 1) for fit I (table 3). The interaction energies for fit II are nearly indistinguishable on this scale. Note that the nearest-neighbor pair interaction J_2 is dominant.

Table 3. Geometric definition of the ‘figures’ F used in our cluster expansion in terms of the vertices of the fcc structure (in units of $\frac{a}{2}$, where a is the lattice parameter). The values of the $T = 0$ cluster interactions $D_F J_F$ for two fits (fit I and fit II) are given in the last two columns. The converged set of interactions is rather insensitive to the structures used to extract them. Negative (positive) J_F denote ferromagnetic (anti-ferromagnetic) interactions.

Cluster type	Designation of figure	Vertices	Value (meV)	
			Fit I	Fit II
Empty	J_0		-43.41	-42.53
Point	J_1	(000)	1.95	2.59
Pairs	J_2	(000),(110)	41.10	41.18
	K_2	(000),(200)	0.71	-0.18
	L_2	(000),(211)	3.65	3.01
	M_2	(000),(220)	-0.48	-1.22
	N_2	(000),(310)	-0.03	
	O_2	(000),(222)	-0.89	
Triplets	J_3	(000),(110),(101)	-0.56	-0.06
	K_3	(000),(110),(200)	-2.22	-3.05
	L_3	(000),(110),(211)	0.89	0.40
Quadruplets	J_4	(000),(110),(101),(011)	-0.31	-0.03

The completely random alloy can alternatively be mimicked using a *single ordered structure* with small number of atoms/cell, the so called special quasirandom structure (SQS) [38, 65] whose spin products $\overline{\Pi}_F$ approximate those of the completely random alloy. The larger the number of atoms in a SQS cell, the closer will SQS mimic completely random alloy. Such special structures have been used previously to model the density of states of random alloys producing results that often agree with experiment but not with valence configuration averaging (VCA) [66] or with coherent potential approximation (CPA) calculations [67].

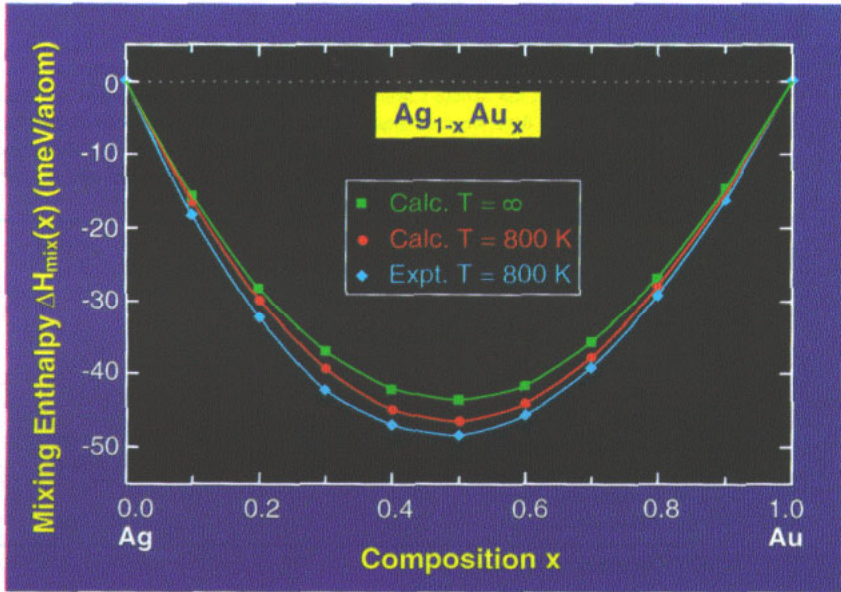


Figure 4. Calculated and measured mixing energy for $\text{Ag}_{1-x}\text{Au}_x$. The measured data (at $T = 800$ K, lozenges) are cited from [23]. We give the calculated values at $T = \infty$ (squares) and 800 K (circles).

Table 4. The experimental [23] and calculated (fit I) $\text{Ag}_{1-x}\text{Au}_x$ mixing enthalpy ΔH_{mix} (meV/atom) using (i) Monte Carlo simulation at $T = 800$ K (including the short-range order effects and (ii) equation (6) corresponding to the completely random alloy ($T \rightarrow \infty$).

x	$\Delta H(x, T = 800 \text{ K})$		$\Delta H(x, T \rightarrow \infty)$
	Expt $T = 800 \text{ K}$	Monte Carlo $T = 800 \text{ K}$	Calc. (equation (6)) $T \rightarrow \infty$
0.0	0.0	0.3	0.3
0.1	-18.2	-16.4	-15.9
0.2	-32.5	-29.8	-28.4
0.3	-42.0	-39.3	-37.0
0.4	-47.1	-44.8	-42.0
0.5	-48.3	-46.4	-43.4
0.6	-45.5	-43.9	-41.3
0.7	-39.1	-37.7	-35.7
0.8	-29.2	-27.9	-26.8
0.9	-16.1	-15.1	-14.7
1.0	0.0	0.4	0.4

At $x = \frac{1}{2}$, one can achieve accurate results with SQS-8, a small cell containing only eight atoms (whose coordinates are given in [38,65]). Indeed, our LDA-calculated $\Delta H(\text{SQS})$ values for Ag–Au

$$\Delta E(\text{SQS8}_a) = -42.5 \text{ meV/atom}$$

and

$$\Delta E(\text{SQS8}_b) = -43.6 \text{ meV/atom}$$

(12)

Table 5. The order-disorder phase transition temperatures T_c for $\text{Ag}_{1-x}\text{Au}_x$ alloys at $x = \frac{1}{4}$, $\frac{1}{2}$, and $\frac{3}{4}$. The calculated results were obtained using N_J interactions, solving the ensuing Ising model with the Monte Carlo (MC) method or with the cluster variation method (CVM). The 'measured' data were obtained by (i) using an inverse Monte Carlo method to extract three composition-dependent effective pair interactions from the short-range order data of the Georgopoulos-Cohen (GC) and Borier-Sparks (BS) analyses and (ii) subjecting the these effective interactions to a direct Monte Carlo simulation.

		Ag ₃ Au L1 ₂	AgAu L1 ₀	AgAu ₃ L1 ₂
Calculated (K)				
Present, fit I	$N_J = 12$; MC	155	210	225
Wei et al ^a	$N_J = 5$; CVM	120	240	200
Mohri et al ^b	$N_J = 5$; CVM	152	177	183
'Measured' (K)				
Schönfeld et al (BS) ^c	$N_J = 3$; MC	115	115	155
Schönfeld et al (GC) ^d	$N_J = 3$; MC	165	165	210
Norman and Warren ^e		90		
Ziesemer ^f			168	

^a Calculated values from [1].

^b Calculated values from [29].

^c Experimentally extracted values from [15] using GC analysis.

^d Experimentally extracted values from [15] using BS analysis.

^e Experimentally extracted values from [40].

^f Experimentally extracted values from [41].

Table 6. Calculated (fit I) and measured real-space SRO parameters $\alpha(R_{lmn}, x)$ (equation (9)) for $\text{Ag}_{1-x}\text{Au}_x$ alloys. The Monte Carlo simulations were done at $T = 600$ K, while the measurements were performed on samples homogenized at ~ 1200 K and then subsequently aged at ~ 500 K. The experimental data were extracted using the Georgopoulos-Cohen (GC, [68]) and Borier-Sparks (BS, [69]) analyses. Note that $\alpha(R_{000}) \equiv 1$. We also give the difference $\delta = \sum |\alpha^{\text{calc}}(R_{lmn}) - \alpha^{\text{expt}}(R_{lmn})|$ (for $R_{lmn} \neq 0$).

Shell		$\alpha(R_{lmn}, x = 0.253)$			$\alpha(R_{lmn}, x = 0.523)$			$\alpha(R_{lmn}, x = 0.750)$		
lmn	R_{lmn}	GC	BS	Theory	GC	BS	Theory	GC	BS	Theory
0 0 0	0.000	1.093	1.145	1.000	1.043	1.190	1.000	1.082	1.090	1.000
1 1 0	0.707	-0.084	-0.072	-0.071	-0.083	-0.081	-0.088	-0.081	-0.068	-0.067
2 0 0	1.000	0.022	0.016	0.016	0.041	0.027	0.039	0.028	0.033	0.027
2 1 1	1.225	0.009	0.009	0.007	0.005	0.009	0.007	0.000	0.005	0.002
2 2 0	1.414	0.012	0.005	0.006	0.017	0.014	0.013	0.038	0.010	0.008
3 1 0	1.581	-0.004	0.005	-0.002	-0.005	-0.008	-0.006	-0.011	-0.005	-0.003
2 2 2	1.732		-0.005	0.002		0.002	0.005		0.004	0.004
3 2 1	1.871			-0.001		-0.002	-0.002		-0.001	-0.001
4 0 0	2.000			0.000		-0.004	0.003		0.002	0.001
3 3 0	2.121			0.000		-0.001	-0.001		-0.010	0.000
4 1 1	2.121			0.001		0.001	0.001			0.000
4 2 0	2.236			0.000		0.003	0.001			0.000
3 3 2	2.345			-0.001		-0.002	-0.001			-0.001
δ		0.029	0.007		0.014	0.024		0.055	0.014	

are within 0.9 meV/atom of values predicted by the the cluster expansion, i.e., -43.4 meV/atom. The latter value was obtained using 18 input structures. This test

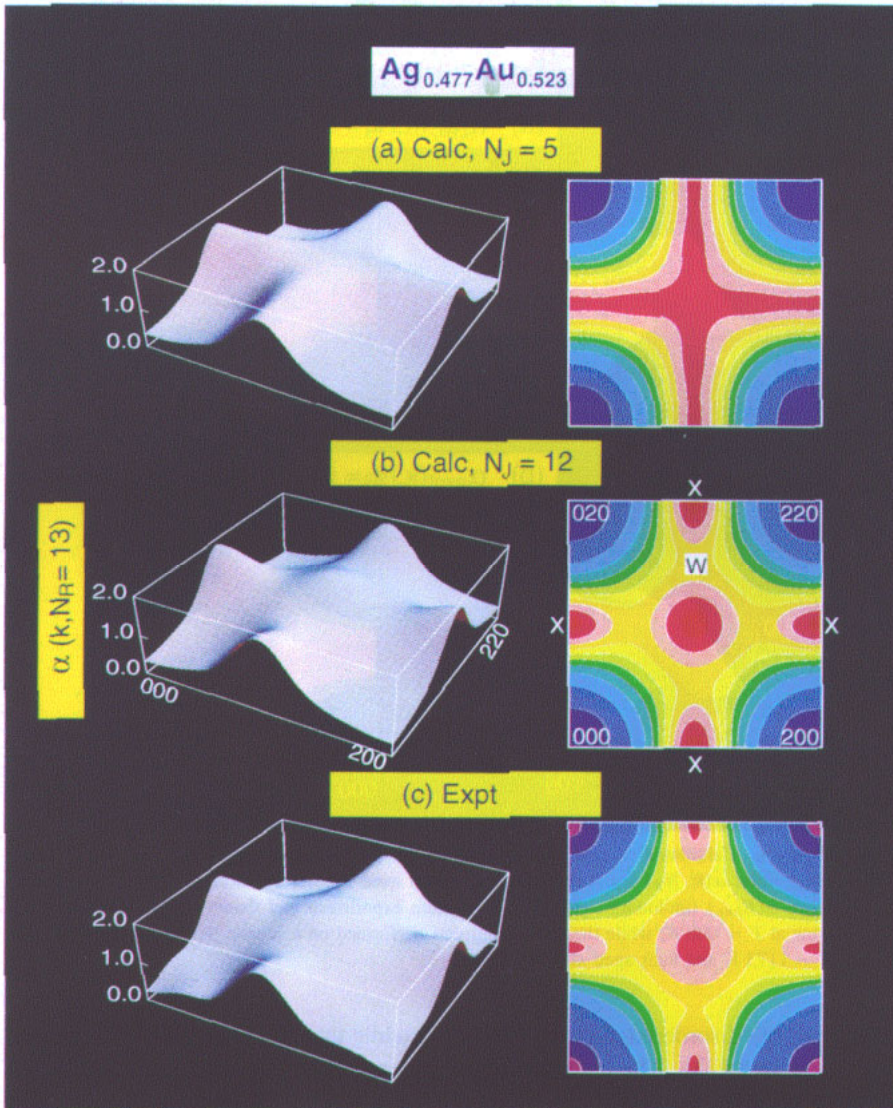


Figure 5. (a) Calculated SRO diffuse-scattering intensity for $\text{Ag}_{1-x}\text{Au}_x$ ($x = 0.5$) using Connolly-Williams set of nearest-neighbor $N_J = 5$ interaction energies, (b) calculated SRO map using our set of $N_J = 12$ interaction energies, and (c) experimental [15] diffuse-scattering intensity due to short-range order $\alpha(\mathbf{k}, N_R)$ for $\text{Ag}_{0.477}\text{Au}_{0.523}$, which were Fourier synthesized using $N_R = 13$ real-space $\alpha(R_{imn})$ (including $\alpha(R_{000}) \equiv 1$ for both experiment and theory). The calculation was done at $T = 600$ K, while the experiment was performed on a sample that was homogenized at $T = 1203$ K and later aged at $T = 502$ K. Note that the intensities in (a) are flat along the X - X lines, where $X = \frac{2\pi}{a} [001]$ (a is the cubic lattice constant) and $W = \frac{2\pi}{a} [0 \frac{1}{2} 1]$ is on the X - X line, while in (b) and (c) there is a pronounced peak at the X point.

confirms the accuracy of SQSs used previously.

The energy of an imperfectly random ('disordered') alloy at finite temperature T can be calculated using the Monte Carlo simulated annealing method. Figure 4 depicts the

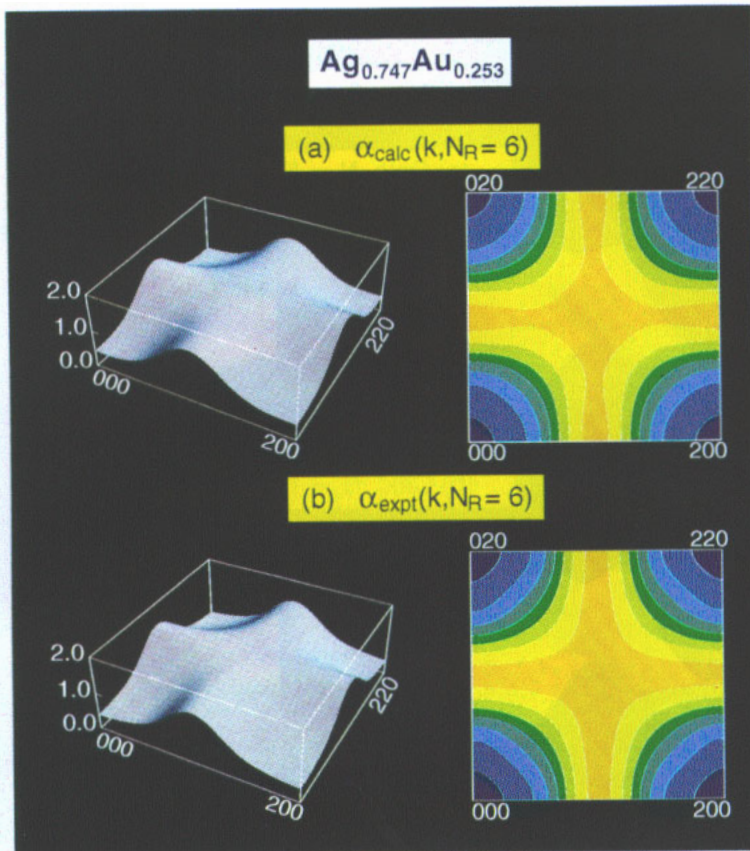


Figure 6. Calculated (a) and experimental (b) [15] diffuse-scattering intensities due to short-range order $\alpha(k, N_R)$ for $\text{Ag}_{0.747}\text{Au}_{0.253}$, which were Fourier synthesized using $N_R = 6$ real-space $\alpha(R_{lmn})$ (including $\alpha(R_{000}) \equiv 1$ for both experiment and theory). The calculation was done at $T = 600$ K, while the experiment was performed on a sample that was homogenized at $T = 1173$ K and later aged at $T = 513$ K.

mixing enthalpy of the disordered alloy at $T = 800$ K while table 4 compares our calculated values with experiment [23]. The agreement is excellent. Note that the finite-temperature enthalpy is more negative than the $T \rightarrow \infty$ values and that the calculated $\Delta H_{\text{mix}}(x, T)$ lie consistently above experiment (by less than 2.7 meV/atom). $\Delta H_{\text{mix}}(x)$ for Ag–Au has also been calculated using empirical methods such as the embedded atom method by Johnson [24] and by Ackland and Vitek [25] and the semiempirical method by Bozzollo and coworkers [26]. These results all agree fairly well with experiment. Terakura and coworkers [27–30] have calculated $\Delta H_{\text{mix}}(x)$ for Ag–Au using the simple five-structure, nearest-neighbor only Connolly–Williams procedure [17], finding also fair agreement with experiment. However, although this simple set of interaction parameter reproduces the $\Delta H_{\text{mix}}(x)$ well, it can not correctly reproduce the shape and composition dependence of the short-range order map $\alpha(\mathbf{k})$, as we will see in section 3.5.

3.4. $T = 0$ ground state structures

The ground state problem can be solved using the linear programming method [61, 62]. For fcc alloys, the most complete searches for the ground state were given by Kanamori and

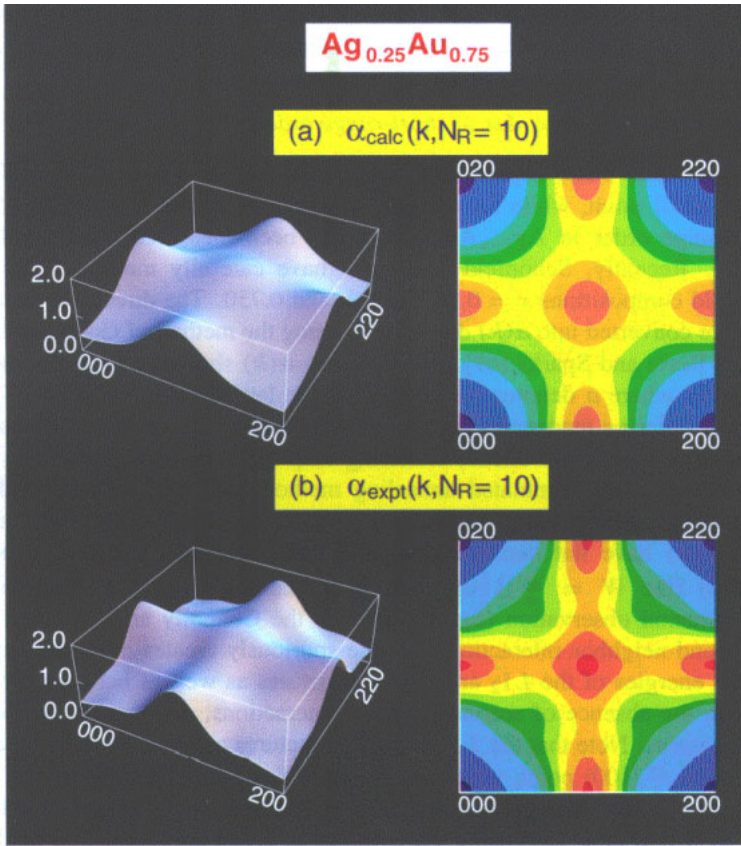


Figure 7. Calculated (a) and experimental (b) [15] diffuse-scattering intensities due to short-range order $\alpha(k, N_R)$ for $\text{Ag}_{0.25}\text{Au}_{0.75}$, which were Fourier synthesized using $N_R = 10$ real-space $\alpha(R_{lmn})$ (including $\alpha(R_{000}) \equiv 1$ for both experiment and theory). The calculation was done at $T = 600$ K, while the experiment was performed on a sample that was homogenized at $T = 1223$ K and later aged at $T = 488$ K.

Takehashi [61] and recently by Garbulsy *et al* [62].

While performing a ground state search using linear programming is relatively easy, it has one drawback: the resulting ground state structure is described in terms of its lattice-averaged products $\overline{\Pi}_F$ which do not always correspond to a physically realizable lattice structure. Here, we will use the Monte Carlo simulated annealing algorithm to perform a ground state search directly on real lattices. This guarantees that the ground state found is always a real structure. The limitation is that one constrains the search to a finite cell, so only structures commensurate with this cell can be obtained. Here we will search the ground state at primary composition of $x = \frac{1}{4}, \frac{1}{2},$ and $\frac{3}{4}$.

The predicted $T = 0$ ground states for $\text{Ag}_{1-x}\text{Au}_x$ are $L_{12}, L_{10},$ and L_{12} , for $x = \frac{1}{4}, \frac{1}{2},$ and $\frac{3}{4}$, respectively. These structures are shown in figure 2. The Monte Carlo simulated annealing also gives the order–disorder phase transition temperature T_c . Table 5 gives our calculated T_c and compares it with other theoretical [1,29] and experimental [15,40,41] estimations. The values of the ‘ordering temperature’ ($T_c < 240$ K) for these compounds are perhaps too low to enable direct growth into the ordered phases (due to slow

atomic diffusion). However, diffuse-scattered intensity due to short-range order at higher temperatures should reveal these ordering tendencies. This is discussed next.

3.5. Diffuse-scattering maps due to short-range order

For a size-matched phase separating system, one expects that $\alpha_{\text{SRO}}(\mathbf{k})$ will show a peak at the $\Gamma = \langle 000 \rangle$ point, while for ordering systems, $\alpha(\mathbf{k})$ will have peaks off the Γ point. The short-range order in $\text{Ag}_{1-x}\text{Au}_x$ alloys has been measured by a number of authors [15, 40, 41]. Recently, Schönfeld *et al* [15] have carefully measured the SRO at three different gold compositions $x = 0.253, 0.523,$ and 0.750 . The directly measured intensities $I_{\text{expt}}(\mathbf{k})$ were converted into $\alpha(\mathbf{k})$ due to SRO using the method of Georgopoulos and Cohen [68] and of Borie and Sparks [69]. The resulting $\alpha(\mathbf{k})$ showed maxima at the wave-vector $X = \frac{2\pi}{a}\langle 100 \rangle$, where a denotes the underlying fcc lattice constant. This off- Γ behavior is indicative of ordering tendencies (i.e., a tendency for having unlike atoms as neighbors).

Figure 5(a) depicts the diffuse-scattering map (at $T = 600$ K and $x = \frac{1}{2}$) calculated using the Monte Carlo simulated annealing method with the Connolly and Williams set of five (nearest-neighbor only) interaction parameters. One immediately notices that the calculated $\alpha(\mathbf{k})$ have flat maxima along the line connecting the two X points $\frac{2\pi}{a}\langle 001 \rangle$ and $\frac{2\pi}{a}\langle 110 \rangle$ (the $W = \frac{2\pi}{a}\langle 1\frac{1}{2}0 \rangle$ point is in the middle), in qualitative contradiction with experimental observation (figure 5(c)). In the Connolly and Williams approach one ignores second-neighbor interactions, so one spuriously creates a degeneracy between the $T = 0$ total energies of the $L1_2$ and DO_{22} structures as well as between the $L1_0$ and '40' structures in the absence of second-neighbor interactions, and this degeneracy survives at high temperatures. Note that the $L1_2$ and $L1_0$ structures are characterized by a reciprocal \mathbf{k} -point, the $X = \frac{2\pi}{a}\langle 100 \rangle$ point, while DO_{22} and '40' are characterized by the $W = \frac{2\pi}{a}\langle 1\frac{1}{2}0 \rangle$ point. Hence one sees flat maxima along the X - W lines. These flat maxima have also been observed by Mohri *et al* [29] using the tetrahedron CVM approximation (and the Connolly and Williams set of interactions). However, Mohri *et al* showed that the flat maxima are lifted if one uses a higher order of configurational entropy, i.e., tetrahedron-octahedron approximation. This is apparently in contradiction with our Monte Carlo results, since we have treated the entropy accurately. We believe that it is the longer-ranged (than nearest neighbor) interactions in Ag-Au that is responsible for lifting this flat maxima. We show next how this flat maxima is lifted in Ag-Au.

This deficiency of resulting flat maxima along the X - W line using the Connolly and Williams procedure was rectified by applying our converged set of interaction parameters. Table 6 gives the calculated and experimental real-space $\alpha(R_{lmn})$. Note that the experimental extracted $\alpha(R_{000})$ deviates from unity, reflecting the degree of uncertainty in their analyses. It appears that $\sum |\alpha^{\text{calc}}(R_{lmn}) - \alpha^{\text{expt}}(R_{lmn})|$ ($R_{lmn} \neq 0$) agrees better with experimental values extracted using the method of Borie and Sparks than that of Georgopoulos and Cohen for $x = 0.253$ and $x = 0.750$ and vice versa for $x = 0.523$. Figures 5-7 compare our calculated diffuse-scattering maps (using our full interaction set) with recent, experimentally determined [15] maps. Our calculated $\alpha_{\text{SRO}}(\mathbf{k})$ agree with experiment fairly well. We see that both calculated and experimental maps have peaks on the X point. The calculated (experimental) peak intensities at the X point are 1.41 (1.41), 1.83 (1.75), and 1.68 (1.60) for $x = 0.253, 0.523,$ and 0.750 , respectively. Note that our calculations reproduce the slight, experimentally observed asymmetry in $\alpha(\mathbf{k})$ with respect to $x = \frac{1}{2}$: there are shallow maxima on the X point in $\alpha(\mathbf{k})$ at $x = 0.253$, while there are relatively pronounced peaks at the X point at $x = 0.750$. This reflects a larger $\Delta H(L1_2) - \Delta E(DO_{22})$ difference at $x = 0.75$ (-3.0 meV/atom) than $x = 0.25$ (-1.1 meV/atom). The $\Delta E(L1_0) - \Delta E('40')$

difference at $x = 0.5$ is -4.4 meV/atom, correlating with a fairly pronounced peak at the X point for $\alpha_{\text{SRO}}(k)$ at $x = 0.523$.

4. Conclusions

We have demonstrated here that accurate alloy properties can be obtained from *ab initio* calculated total energies of ~ 20 simple structures coupled with a generalized Ising model (including pair and many-body interactions) and statistical mechanics. We show that a converged expansion can be achieved by including relatively short-ranged interactions for the Ag–Au alloy system. We find that the $\text{Ag}_{1-x}\text{Au}_x$ alloy system will order into $L1_2$, $L1_0$, and $L1_2$ structures at $x = \frac{1}{4}$, $x = \frac{1}{2}$, and $x = \frac{3}{4}$, respectively. Although the ordering temperatures are too low to enable direct growth into ordered phases, the calculated and experimental diffuse-scattering intensities at high temperatures indeed indicate these ordering propensities. The calculated mixing energy and short-range order parameters for Ag–Au agree quantitatively with experiment.

Acknowledgments

ZWL and BMK thank the University Research Funds of the University of California at Davis for support. AZ thanks the Office of Energy Research (OER) (Division of Materials Science of the Office of Basic Sciences (BES)), US Department of Energy, for support under contract No DE-AC36-83CH10093.

References

- [1] Wei S-H, Mbaye A A, Ferreira L G and Zunger A 1987 *Phys. Rev. B* **36** 4163
- [2] Ferreira L G, Wei S-H and Zunger A 1989 *Phys. Rev. B* **40** 3197
- [3] Wei S-H, Ferreira L G and Zunger A 1990 *Phys. Rev. B* **41** 8240
- [4] Lu Z W, Wei S-H and Zunger A 1991 *Phys. Rev. Lett.* **66** 1753–6
- [5] Lu Z W, Wei S-H, Zunger A, Frota-Pessoa S and Ferreira L G 1991 *Phys. Rev. B* **44** 512
- [6] Wolverton C, Ceder G, de Fontaine D and Dreyssé H 1993 *Phys. Rev. B* **48** 726
- [7] Lu Z W, Wei S-H, and Zunger A 1993 *Europhys. Lett.* **21** 221–6
- [8] Lu Z W, Klein B M and Zunger A 1995 *J. Phase Equilibria* **16** 36
- [9] Lu Z W, Klein B M and Zunger A 1995 *Phys. Rev. Lett.* **75** 1320–3
- [10] Lu Z W and Zunger A 1994 *Phys. Rev. B* **50** 6626
- [11] Zunger A 1993 *Statics and Dynamics of Alloy Phase Transitions (NATO ASI Series)* ed P E A Turchi and A Gonis (Dordrecht: Kluwer)
- [12] de Fontaine D *Solid State Physics* ed H Ehrenreich and D Turnbull (New York: Academic) at press
- [13] Domb C 1974 *Phase Transition and Critical Phenomena* vol 3, ed C Domb and H S Green (London: Academic) p 357
- [14] Dahmani C E, Cadeville M C, Sanchez J M and Morán-López J L 1985 *Phys. Rev. Lett.* **55** 1208
- [15] Schönfeld B, Traube J and Kistorz G 1992 *Phys. Rev. B* **45** 613
- [16] Solal F, Caudron R, Ducastelle F, Finel A and Loiseau A 1987 *Phys. Rev. Lett.* **58** 2245
- [17] Connolly J W D and Williams A R 1983 *Phys. Rev. B* **27** 5169
- [18] Hohenberg P and Kohn W 1964 *Phys. Rev. B* **136** 864
Kohn W and Sham L J 1965 *Phys. Rev. A* **140** 1133
- [19] Laks D B, Ferreira L G, Froyen S and Zunger A 1992 *Phys. Rev. B* **46** 12587
- [20] de Gironcoli S, Giannozzi P and Baroni S 1991 *Phys. Rev. Lett.* **66** 2116
- [21] Beiden S V and Vaks V G 1992 *Phys. Lett.* **163A** 209
- [22] Lu Z-W, Laks D B, Wei S-H and Zunger A 1994 *Phys. Rev. B* **50** 6642
- [23] White J L, Orr R L and Hultgren R 1957 *Acta Metall.* **5** 747
- [24] Johnson R A 1989 *Phys. Rev. B* **39** 12554–9; 1990 *Phys. Rev. B* **41** 9717–20
- [25] Ackland G J and Vitek V 1990 *Phys. Rev. B* **41** 10324–33

- [26] Bozzolo G, Ferrante J and Smith J R 1992 *Phys. Rev. B* **45** 493
- [27] Terakura K, Oguchi T, Mohri T and Watanabe K 1987 *Phys. Rev. B* **35** 2169–73
- [28] Mohri T, Terakura K, Oguchi T and Watanabe K 1988 *Acta Metall. Mater.* **36** 547–53
- [29] Mohri T, Terakura K, Takizawa S and Sanchez J M 1991 *Acta Metall. Mater.* **39** 493–501
- [30] Mohri T, Takizawa S and Terakura K 1993 *J. Phys.: Condens. Matter* **5** 1473–80
- [31] Watson R E, Hudis J and Perlman M L 1971 *Phys. Rev. B* **4** 4139
- [32] Fain S C and McDavid J M 1974 *Phys. Rev. B* **9** 5089
- [33] Wu S C, Wang Z Q, Sondericker D, Sokolov J, Garrett R F and Jona F 1986 *Phys. Rev. B* **34** 8418
- [34] Sham T K, Bzowski A, Kuhn M and Tyson C C 1990 *Solid State Commun.* **80** 29
Tyson C C, Bzowski A, Kristof P, Kuhn M, Sammynaiken R and Sham T K 1992 *Phys. Rev. B* **45** 8924
- [35] Levin K and Ehrenreich H 1971 *Phys. Rev. B* **3** 4172
- [36] Gelatt C D and Ehrenreich H 1974 *Phys. Rev. B* **10** 398
- [37] Ebert H, Weinberger P and Voitländer J 1986 *Z. Phys. B* **63** 299
- [38] Lu Z W, Wei S-H and Zunger A 1991 *Phys. Rev. B* **44** 10470
- [39] Klein B M and Fong C Y 1994 *Metallic Alloys: Experimental and Theoretical Perspectives* ed J S Faulkner and R G Jordan (Dordrecht: Kluwer) p 291
- [40] Norman N and Warren B E 1951 *J. Appl. Phys.* **22** 483
- [41] Ziesemer K 1976 *PhD Thesis* Universität Frankfurt
- [42] Miller T, Samsavar A, Franklin G E and Chiang T-C 1988 *Phys. Rev. Lett.* **61** 1404
- [43] Lindgren S Å and Walldén L 1989 *J. Phys.: Condens. Matter* **1** 2151
- [44] Miller T and Chiang T-C 1992 *Phys. Rev. Lett.* **68** 3339
- [45] McMahon W E, Miller T and Chiang T-C 1993 *Phys. Rev. Lett.* **71** 907
- [46] Corcoran S G, Chakarova G S and Sieradzki K 1993 *Phys. Rev. Lett.* **71** 1585
- [47] Chan C T, Bohnen K P and Ho K M 1992 *Phys. Rev. Lett.* **69** 1672
- [48] Wyckoff R W G 1963 *Crystal Structures* (New York: Wiley)
- [49] Metropolis N, Rosenbluth A W, Rosenbluth M N, Teller A H and Teller E 1953 *J. Chem. Phys.* **21** 1087
- [50] Binder K and Heermann D W 1988 *Monte Carlo Simulations in Statistical Physics* (Berlin: Springer)
- [51] Binder K (ed) 1992 *The Monte Carlo Method in Condensed Matter Physics* (Berlin: Springer)
- [52] Kirkpatrick S, Gelatt C D Jr and Vecchi M P 1983 *Science* **220** 671
- [53] Sanchez J M, Ducastelle F and Gratias D 1984 *Physica A* **128** 334
Sanchez J M 1993 *Phys. Rev. B* **48** 14013
- [54] Andersen O K 1975 *Phys. Rev. B* **12** 3060
Wimmer E, Krakauer H, Weinert M and Freeman A J 1981 *Phys. Rev. B* **24** 864
Hamann D R 1979 *Phys. Rev. Lett.* **42** 662
Wei S-H and Krakauer H 1985 *Phys. Rev. Lett.* **55** 1200
Wei S-H, Krakauer H and Weinert M 1985 *Phys. Rev. B* **32** 7792
- [55] Singh D J 1994 *Planewaves, Pseudopotentials, and the LAPW Method* (Boston, MA: Kluwer)
- [56] Ceperley D M and Alder B J 1980 *Phys. Rev. Lett.* **45** 566
- [57] Perdew J P and Zunger A 1981 *Phys. Rev. B* **23** 5048
- [58] Monkhorst H J and Pack J D 1976 *Phys. Rev. B* **13** 5188
- [59] Wigner E 1934 *Phys. Rev.* **46** 1002
- [60] Froyen S 1989 *Phys. Rev. B* **39** 3168
- [61] Kanamori J and Kakehashi Y 1977 *J. Physique* **38** 274
- [62] Garbulsky G D, Tapesch P D and Ceder G 1993 *Materials Theory and Modelling Symposium* ed J Broughton, P Bristowe and J Newsam (Pittsburgh, PA: Materials Research Society) pp 259–65
- [63] Cowley J M 1950 *J. Appl. Phys.* **21** 24
- [64] Warren B E 1990 *X-ray Diffraction* (New York: Dover)
- [65] Zunger A, Wei S-H, Ferreira L G and Bernard J E 1990 *Phys. Rev. Lett.* **65** 352
Wei S-H, Ferreira L G, Bernard J E and Zunger A 1990 *Phys. Rev. B* **42** 9622
Wei S-H and Zunger A 1991 *Phys. Rev. B* **43** 1662
- [66] Magri R, Froyen S and Zunger A 1991 *Phys. Rev. B* **44** 7947
- [67] Lu Z W, Wei S-H and Zunger A 1991 *Phys. Rev. B* **44** 3387; 1992 *Phys. Rev. B* **45** 10314
- [68] Georgopoulos P and Cohen J B 1977 *J. Physique Coll.* **38** C7 191
- [69] Borie B and Sparks C J 1971 *Acta Crystallogr. A* **27** 198